Ceramics International 44 (2018) 17767–17774

Contents lists available at ScienceDirect

Ceramics International

journal homepage: www.elsevier.com/locate/ceramint

Structural, magnetic and optical investigations of Fe and Ni co-doped TiO_2 dilute magnetic semiconductors

Salma Waseem[a,*], Safia Anjum[a], Lubna Mustafa[a], Tallat Zeeshan[a], Zohra Nazir Kayani[a], Khalid Javed[b]

[a] Department of Physics, Lahore College for Women University, Lahore, Pakistan
[b] Department of Physics, Forman Christian college, Lahore, Pakistan

ARTICLE INFO

Keywords:
Rutile
Transition metals
Band gap energy
Ferromagnetization

ABSTRACT

A series of $Ti_{0.9}Fe_{0.1-x}Ni_xO_2$ (x = 0.0, 0.02, 0.04, 0.06, 0.08, 0.1) has been synthesized through the solid state reaction method at annealing temperature of 1100 °C for two hours. The synthesized samples have been analyzed by X-Ray diffractometer (XRD), Raman spectroscopy, Scanning electron microscopy (SEM), Energy dispersive X-ray spectroscopy (EDX), Vibrating sample magnetometer (VSM) and ultraviolet visible (UV–VIS) spectroscopy for structural investigations, defects measurements, surface morphology, magnetic and optical properties respectively. Structural analysis has revealed the dominant structure of rutile. An intensity loss and peak broadening of TiO_2 (rutile) vibration lines have been observed from Raman analysis, which is an indication of presence of oxygen vacancies. Magnetic analysis has revealed ferromagnetic behavior at room temperature. Optical characterization has shown the blue shift in band gap energy with increase of Ni concentration.

1. Introduction

Since the last decade, dilute magnetic semiconductors (DMS) have attracted much attention of the research community because of their widespread applications in spintronics [1]. DMS are obtained by the doping of magnetic transition metals like Co, Fe and Mn etc. into non-magnetic semiconductors. It is one of the most important topics in the spintronics field which is analogous to the traditional semiconductor electronics [2]. Since the theoretical work done by Dietl. et al. in 2000 [3,4], wide band gap semiconductors (TiO_2, ZnO, TiO_2) are considered the most promising candidates for obtaining room temperature ferromagnetic behavior. Matsumoto et al. in 2000 investigated Co doped TiO_2 for obtaining room temperature ferromagnetic behavior and opened a new vista into the spintronics industry [5].

Among oxide dilute magnetic semiconductors TiO_2 is very important because of its usage in various industrial fields due to its exceptional electrical and magnetic properties. It is used as a white pigment in sunscreen and paint because of its high refractive index [6,7]. It has been widely studied for treatment of waste water [8–10], corrosion-protective coatings [11], bone implants [12,13], spin valve memristive systems [14–16], electrochromical devices [14–16], Li-based batteries [17–19] and dye sensitized solar cells [20].

Transition metals doped in TiO_2 have been prepared through various techniques like wet chemical synthesis [21], sol–gel method [22], thermal hydrolysis [23], sonochemical route [24], RF plasma synthesis from metal mixtures [25] and oxidative pyrolysis of organo metallic precursors in induction thermal plasma [26], ion-implantation [27], ion beam induced chemical vapor deposition (IBICVD) [28].

However the ferromagnetism depends strongly upon synthesis methods and experimental conditions. Tseng, L.T. et al. [29] synthesized TiO_2 nanorods with doping of different transition metals (Ni, Co, Fe and Mn) by the molten state method. It was observed that doping of different transition metal ions into TiO_2 gave rise to paramagnetic behavior instead of ferromagnetic behavior. Li, M. et al. [30] synthesized vanadium (V) doped TiO_2 microspheres by co-precipitation method with the help of Ti and V precursors. Vanadium was incorporated into TiO_2 homogeneously which promoted the transition of TiO_2 from anatase to rutile phase. TiO_2 doped with V displayed room temperature ferromagnetic behavior. The obtained magnetization was associated mainly with structural defects.

As far as the source of ferromagnetization in DMS is concerned, it is still a controversial issue [31]. However, there are four factors which are considered the source of ferromagnetization i.e. (i) oxygen vacancies (ii) transition metal dopants (iii) cation vacancies and (iv) the change of titanium oxidation state (Ti^{3+}). The oxygen vacancies cause a noticeable change in band structure which is the major cause of

* Corresponding author.
E-mail address: salma_iqbal1990@hotmail.com (S. Waseem).

https://doi.org/10.1016/j.ceramint.2018.06.244
Received 9 February 2018; Received in revised form 21 April 2018; Accepted 28 June 2018
Available online 04 July 2018

ferromagnetization. while transition metals have unpaired d electrons which induce the magnetic moment to DMS [32,33]. An important parameter of DMS is accurate adjustment of different types of exchange interactions like s, p-band and d-band electrons by the doping of different types of transition metals without changing their structure [34].

In this project Fe and Ni are co-doped into TiO_2 because previous research has shown that two dopants have a more synergistic effect than one, with respect to the increasing absorption in the visible light region [35,36]. Moreover better magnetic and electrical properties can be achieved, if two transition metals are co-doped with TiO_2 [37]. Fe^{+2} is considered a very appropriate candidate for doping. Fe^{2+} might easily be incorporated within the crystal lattice of TiO_2 [38]. Fe-doped TiO_2 is of great interest due to its potential applications in magneto-optic devices and spintronics [39,40]. On the other hand Ni doped into TiO_2 shows complications in room temperature ferromagnetic behavior [41]. Zhao et al. found that doping of Ni in TiO_2 induced reversible ferromagnetism [42] while, Bahadur et al.reported that with an increase of Ni contents, the magnetization of TiO_2 powders decreased which was attributed to oxygen vacancies destroying spin order. Therefore more experimental investigations are required in order to fully understand the mechanism of ferromagnetization in Ni doped TiO_2 [43].

To the best of our knowledge Fe and Ni are co-doped into TiO_2 first time by the solid state reaction method. It is seen that most of the work on TiO_2 based DMS has been done either on thin films or on the synthesis of nanoparticles through chemical route; a little attention has been paid on the synthesis of TiO_2 based DMS by the solid state reaction method. Moreover, there is a little research work on co-doped TiO_2 as compared to single doped TiO_2. Here an attempt has been made to synthesize Fe and Ni co-doped TiO_2 in order to tune the optical and the magnetic properties at room temperature.

2. Materials and methods

A series of $Ti_{0.9}Fe_{0.1-x}Ni_xO_2$ (x = 0.00, 0.02, 0.04, 0.06, 0.08 and 0.10) was prepared by a simple and low cost solid state reaction method. The flowchart of solid state reaction method is shown in Fig. 1. All the powder samples were weighed according to their stoichometric ratio by using a precise electronic balance. After weighing, all the powder samples were mixed and ground individually for six hours using Ceramic Mortar and Pestle to get homogenous mixture. These raw samples were calcined in an air furnace at 1100 °C for two hours. After heat treatment, the samples were again reground for two hours and mixed thoroughly. The samples were used to make pallets of 1 cm diameter by applying a pressure of 3 tons in a Hydraulic press. These pallets were sintered at 650 °C for two hours for the purpose of hardening.

In this work, Crystal structure and phase identification of the samples were examined using X-ray diffractometer D-8 discover, Bruker, made in Germany, having source Cu-Kα radiations with the wavelength 1.54 Å. A Bruker Optics (Billerica, MA) Senterra microscope spectrometer was used for Raman spectroscopy analysis. The Surface morphology of the samples was observed through scanning electron microscope (SEM) using S-3400N Hitachi. Room temperature magnetic measurements were performed by Lakeshore 7436 vibrating sample magnetometer. The samples were examined optically by using UV 2800 model, Hitachi Japan, with wavelength 300–900 nm.

3. Results and discussion

3.1. XRD analysis

The comparative XRD patterns of the series $Ti_{0.9}Fe_{0.1-x}Ni_xO_2$ (x = 0, 0.02, 0.04, 0.06, 0.08 and 0.10) are shown in Fig. 2(a). All the peaks occurring at 27.39°, 35.86°, 39.18°, 41.26°, 44.03°, 54.27°, 56.7°, 62.42°, 63.98° and 69.1° have been attributed to (110), (101), (200), (111), (210), (211), (210), (002), (310) and (301) planes after matching the peaks with JCPDS card No 21-1272 [44]. The true rutile phase of TiO_2 has been observed. There is not a single peak belonging to Anatase or the orthorhombic phase of TiO_2. Moreover, the secondary peaks belonging to oxides of Fe or Ni like Fe_2O_3, Fe_3O_4 and NiO are absent which depict the highly pure, single phase, polycrystalline rutile structure of the prepared samples. It is observed from the diffraction patterns that all the samples are preferably growing along (110) direction. The intensity of the peaks increases with increasing Ni concentration which is responsible for the high crystallinity of the samples.

The rutile lattice constants ***a*** and ***c*** have been calculated by taking into account the highest intensity diffraction peak (110) and its neighboring peak (101) using the relation given below [45].

$$\frac{1}{d^2} = \frac{h^2 + k^2}{a^2} + \frac{l^2}{c^2} \quad (1)$$

where (***h, k, l***) are miller indices of corresponding plane, ***d*** is interplanar spacing. The calculated values of lattice constants ***a*** and ***c*** with

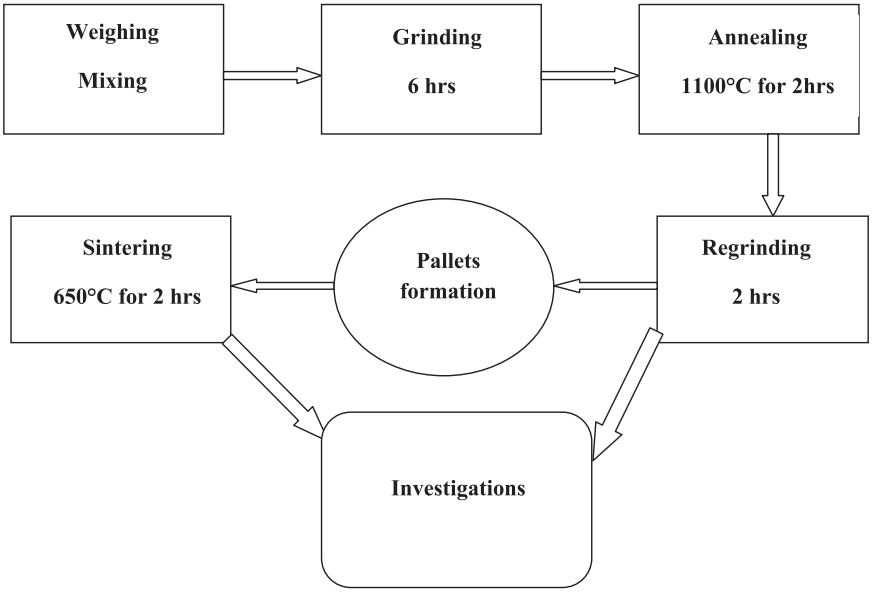

Fig. 1. Flow chart of solid state reaction method.

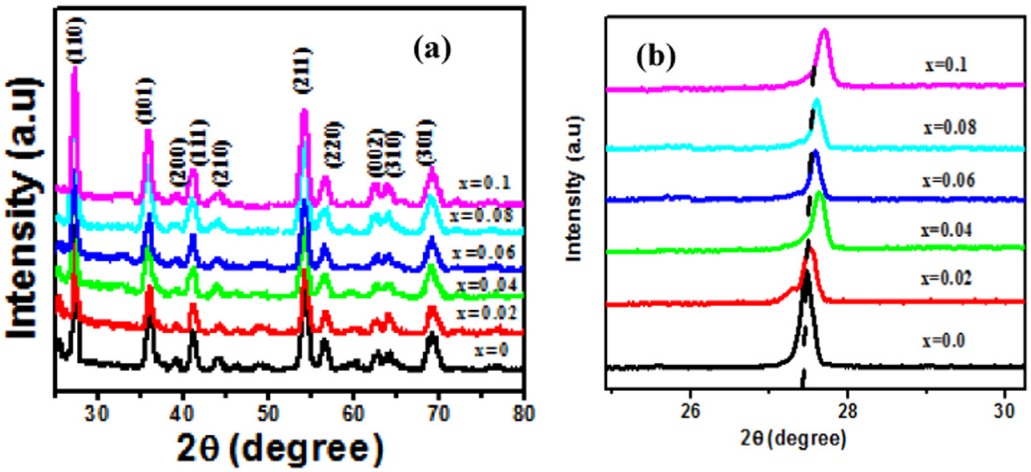

Fig. 2. (a): Comparative XRD patterns of $Ti_{0.9}F_{0.1-x}Ni_xO_2$ **(b):** magnified view of the highest intensity (110) peak.

Table 1
XRD parameters of $Ti_{0.9}Fe_{0.1-x}Ni_xO_2$.

Composition (x)	Crystallite size (D) (nm)	Lattice constant a (A°)	Lattice constant c (A°)	Lattice strain $\times 10^{-3}$	Dislocatin density (ε) $\times 10^{-3}$
$Ti_{0.9}Fe_{0.1}O_2$	22.86	4.598	2.963	8.8	1.91
$Ti_{0.9}Fe_{0.08}Ni_{0.02}O_2$	17.45	4.598	2.963	10.2	3.28
$Ti_{0.9}Fe_{0.06}Ni_{0.04}O_2$	15.05	4.595	2.939	10.4	4.41
$Ti_{0.9}Fe_{0.04}Ni_{0.06}O_2$	14.73	4.584	2.937	13.6	4.61
$Ti_{0.9}Fe_{0.02}Ni_{0.08}O_2$	13.99	4.583	2.926	14.4	5.11
$Ti_{0.9}Ni_{0.1}O_2$	13.33	4.572	2.924	17.4	5.63

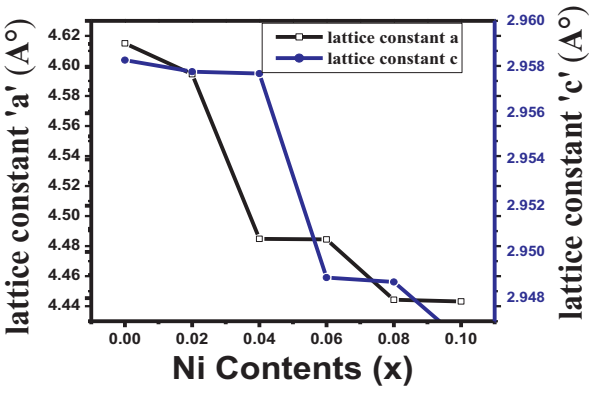

Fig. 3. The Variation of lattice constants of $Ti_{0.9}Fe_{0.1-x}Ni_xO_2$ with Ni contents.

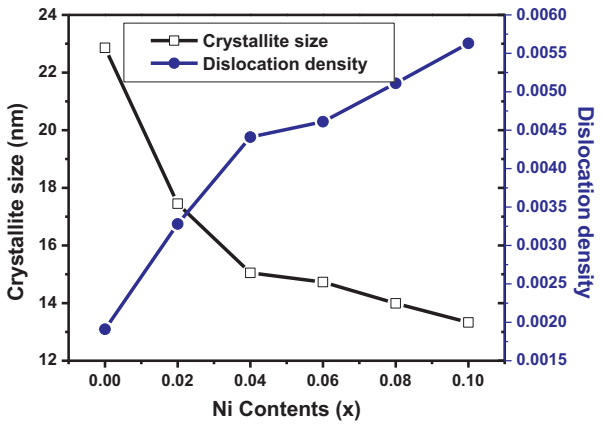

Fig. 4. The variation of crystallite size and dislocation density of $Ti_{0.9}Fe_{0.1-x}Ni_xO_2$ with Ni contents.

varying concentration of x are tabulated in Table 1. The relationship between a and c as a function of Ni concentration is shown in Fig. 3. It is noticed that as Ni concentration increases into $Ti_{0.9}Fe_{0.1}O_2$ host, lattice constants ***a*** and **c** both decrease. It may be due to incorporation of smaller ionic radius of substituent, Ni^{+2} (0.69 A°) than host Fe^{2+} (0.75 A°) into TiO_2 [46,47]. These results agree well with the earlier findings [48,49]. The magnified view of the most intense diffraction peak (110) is shown in Fig. 2(b). It is observed that the peak is shifted slightly towards higher angle as Ni is doped into $Ti_{0.9}Fe_{0.1}O_2$. This shifting may occur due to the stress produced in the structure as a result of the shrinkage of unit cell because of the difference of ionic radii of Fe^{+2} and Ni^{+2} [50].

The crystallite size (D) is evaluated by well known Debye Scherrer's formula, given below [51].

$$D = k\lambda/\beta \, Cos\, \theta \quad (2)$$

A decrease in crystallite size is observed with increasing the Ni concentration. This result is similar to one reported earlier [52]. The variation of crystallite size as a function of Ni contents is shown in Fig. 4.

The strain ***ε*** present in lattice due to imperfections and distortions is estimated by the following relation [53].

$$\varepsilon = \beta/4 \tan \theta \quad (3)$$

The value of strain is 8.8×10^{-3} for $Ti_{0.9}Fe_{0.1}O_2$ which keeps on increasing with the addition of Ni contents. It increases from 8.8×10^{-3} to 1.74×10^{-2}. This increase in strain with increasing Ni contents may be co-related to decrease in crystallite size [54]. The dislocation line density ***δ*** is computed by the relation given below [46].

$$\delta = 1/D^2 \quad (4)$$

The dislocation line density is increasing by increasing Ni contents. The variation of crystallite size and dislocation line density as a function of Ni contents are represented in Fig. 4.

The values of lattice strain, crystallite size and dislocation line density are tabulated in Table 1.

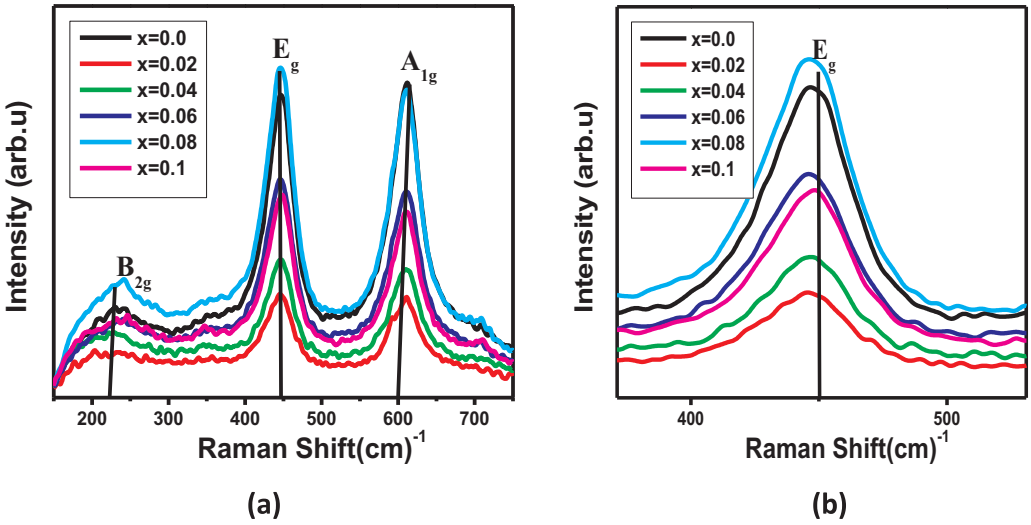

Fig. 5. (a): Raman spectrum of $Ti_{0.9}Fe_{0.1-x}Ni_xO_2$ **(b)** Magnified view of most intense Raman mode E_g.

3.2. Raman spectroscopy analysis

The Raman analysis of $Ti_{0.9}Fe_{0.1-x}Ni_xO_2$ is carried out at room temperature and raman spectra of $Ti_{0.9}Fe_{0.1-x}Ni_xO_2$ (x = 0.0, 0.02, 0.04, 0.06, 0.08, 0.1) are shown in Fig. 5. The rutile phase exhibits major peaks at 610, 446, and 242 cm^{-1} and minor peaks at 818, 707, and 319 cm^{-1}[55]. From the spectra, it is observed that there are three major peaks present i.e. at 264, 415 and 608 cm^{-1} which confirms the formation of rutile phase of TiO_2. Usually the four active Raman vibration modes of rutile phase are given by the following equation.

$$A_{1g} + B_{1g} + B_{2g} + Eg \quad (5)$$

The peaks ranging from 446 to 452 cm^{-1} belong to $\boldsymbol{E_g}$ mode, whereas the peaks ranging from 612 to 623 belong to $\boldsymbol{A_{1g}}$ mode. The peaks at 240–264 cm^{-1} belong to $\boldsymbol{B_{2g}}$ mode and are known as compound vibration peaks due to multiple phonon scattering process. This mode is known as Characteristic Raman mode of rutile TiO_2 [56,57]. This mode is broad and weak due to phonon confinement effect.

It is observed that when Ni is doped into $Ti_{0.9}Fe_{0.1}O_2$, the intensity of all the observed Raman bands decreases while their width increases. The decrease in intensity of $\boldsymbol{A_{1g}}$ mode is due to creation of Ni- Ti-O clusters as well as defects in the lattice. The E_g mode is quite sensitive to oxygen vacancies in Ti^{3+}. The decline in the intensity of this mode reveals the reduction in TiO_2 lattice stoichiometry [58]. The decrease in the intensity of $\boldsymbol{B_{2g}}$ mode may be due to difference of ionic radius of Fe^{+2} (0.75 A°), Ni^{+2} [0.69 A°] and Ti^{+4} [0.68 A°]. It is observed that as the Ni contents increase, there is a frequency shift of Raman modes. $\boldsymbol{E_g}$ and $\boldsymbol{A_{1g}}$ mode are blue shifted while $\boldsymbol{B_{2g}}$ mode is red shifted. This shifting of Raman modes may be due to lattice strain. Moreover crystallize size and defects also affect the shifting and broadening of Raman modes [59]. The observed values of Raman shift of different modes are tabulated in Table 2.

Table 2
Variation of Raman modes of $Ti_{0.9}Fe_{0.1-x}Ni_xO_2$ with Ni contents.

Composition	$B_{2g}(cm)^{-1}$	E_g $(cm)^{-1}$	E_{1g} $(cm)^{-1}$
$Ti_{0.9}Fe_{0.1}O_2$	240	446	612
$Ti_{0.9}Fe_{0.08}Ni_{0.02}O_2$	238	446	613
$Ti_{0.9}Fe_{0.06}Ni_{0.04}O_2$	237	447	614
$Ti_{0.9}Fe_{0.04}Ni_{0.06}O_2$	237	449	615
$Ti_{0.9}Fe_{0.02}Ni_{0.08}O_2$	229	450	616
$Ti_{0.9}Ni_{0.1}O_2$	226	452	623

3.3. SEM analysis

The SEM micrographs of $Ti_{0.9}Fe_{0.1-x}Ni_xO_2$ (x = 0.0, 0.02, 0.04, 0.06, 0.08, 0.1) are shown in Fig. 6. The Ni free sample ($Ti_{0.9}Fe_{0.1}O_2$) shows agglomeration of smaller grains which increase in size as the concentration of Ni increases. The agglomeration of the grains may be due to high surface energy and the appearance of nanometer size grains with good surface coverage [60]. The Ni free sample also shows a greater number of voids which decrease as the concentration of Ni increases. However, all the samples show denser, inhomogeneous and congested surfaces, with the continuous appearance of nanograins. No cracks are observed. A modified surface is observed with increasing Ni contents.

From these micrographs grain sizes are evaluated by the linear fit method whose values are tabulated in Table 4. It is observed that grain size increases with increasing the concentration of Ni ions in $Ti_{0.9}Fe_{0.1}O_2$.

3.4. EDX analysis

The elemental analysis of all the samples of $Ti_{0.9}Fe_{0.1-x}Ni_xO_2$ (x = 0.0, 0.02, 0.04, 0.06, 0.08, 0.1) is shown in Fig. 7. It shows that the concentration of Fe and Ni is in accordance with the stoichometric ratio in $Ti_{0.9}Fe_{0.1-x}Ni_xO_2$.

3.5. VSM analysis

The magnetic properties of$Ti_{0.9}Fe_{0.1-x}Ni_xO_2$ have been studied at room temperature by applying a magnetic field of 2 T. Hysteresis (M-H) loops of $Ti_{0.9}Fe_{0.1-x}Ni_xO_2$ (x = 0.0, 0.02, 0.04, 0.06, 0.08, 0.1) are shown in Fig. 8. The different parameters like magnetization (***M***), retentivity (***Mr***), coercivity (***Hc***) are extracted from the hysteresis loop and are tabulated in Table 3. All the samples have magnetization at zero magnetic field and also have some coercivity which confirms the ferromagnetic nature of the samples [61]. It shows that as the Ni contents are doped into $Ti_{0.9}Fe_{0.1}O_2$, magnetization decreases from 0.27 emu/g to 0.07 emu/g. The decrease in magnetization may be due to less magnetic moment of doped atom Ni^{+2} (2 μ_B) than host Fe^{+2} (5 μ_B) atom. The decrease in magnetization with an increase in Ni contents is shown in the inset of Fig. 8. On the other hand coercivity increases from 33 to 99 Oe with an increase in Ni contents and then decreases in the last sample ($Ti_{0.9}Ni_{0.1}O_2$), in the absence of Fe. This increase in coercivity can be attributed to the collective effect of two magnetic impurities (Fe and Ni) giving rise to strong ferromagnetic coupling [46].

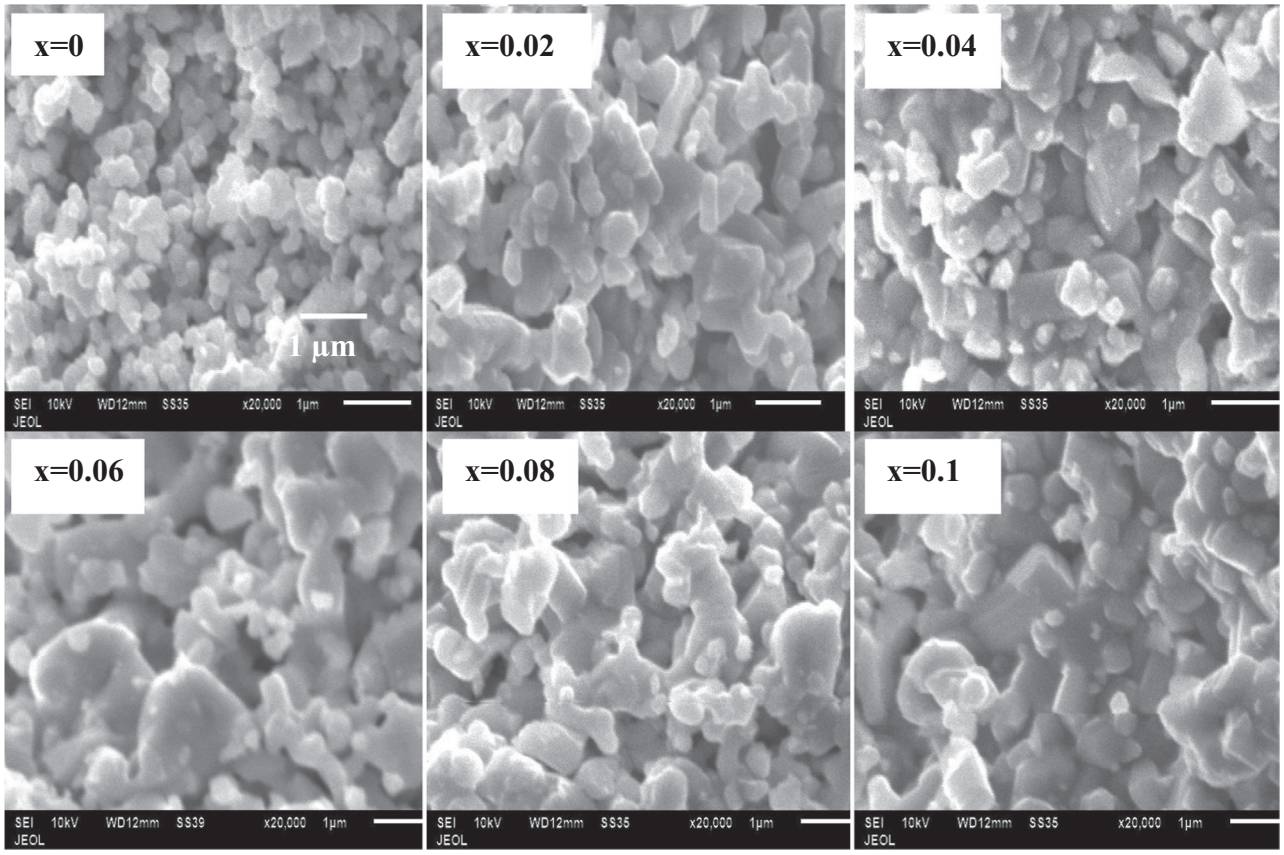

Fig. 6. SEM micrographs of $Ti_{0.9}Fe_{0.1-x}Ni_xO_2$.

The origin of ferromagnetism has always been a controversial issue because of different conflicting magnetic sources discussed in literature. The source of magnetic behavior is complicated and is dependent on a number of parameters like dopant type, carrier density and spacing between magnetic ions. These factors affect the electronic band structure of dilute magnetic semiconductors which in turn affects its magnetic properties.

One of sources of ferromagnetization is secondary phases or extrinsic origin [43]. In the present research work there is no possibility of ferromagnetization due to extrinsic origin like Ni clusters or oxides of Ni or Fe as is confirmed from XRD patterns of $Ti_{0.9}Fe_{0.1-x}Ni_xO_2$. Another cause of ferromagnetism in DMS is super-exchange d-d interactions which enhance with the increase in dopant contents [46]. So the increase in dopant contents should increase the magnetization, but here a reverse trend is observed, where a decrease in magnetization is observed by an increase in Ni contents. Hence this source of ferromagnetization is also not affective here.

The other cause of ferromagnetization may be the indirect exchange interactions (RKKY model) in which the Ni^{+2} ions may be ferromagnetically aligned via free carriers. Our XRD results show that when Ni is doped into TiO_2-Fe, a true rutile phase is observed with a linear decrease in crystallite size. The magnetization also decreases as is obvious from Table 2. So the RKKY model may be applicable here [62].

One of the possibilities may be the presence of oxygen vacancies which are formed in order to compensate for charge neutrality when Ti^{+4} is replaced by Ni^{+2} [62]. Oxygen vacancies are also formed during annealing in solid state reaction method. It is already reported [62] that TiO_2 shows strong polaronic effect in which the effective mass of carriers becomes larger due to electron phonon interaction. As a result, the polaronic electron spends most of its time close to an oxygen vacancy. When this electron is trapped by an oxygen vacancy, F center is generated. The trapped electron with an orbital overlaps with the d shell of magnetic impurities. Therefore a F- center bound magnetic polaron can also be the cause of ferromagnetization here. The ferromagnetism is attained when a number of magnetic polarons start overlapping and form a constant chain through the whole material. In this way ferromagnetism is percolated in DMS [63].

3.6. UV–VIS analysis

The optical properties of $Ti_{0.9}Fe_{0-1-x}Ni_xO_2$ are studied by UV–Vis spectrophotometer at room temperature. The UV–Vis absorbance spectra of $Ti_{0.9}Fe_{0-1-x}Ni_xO_2$ is presented in Fig. 9. It is observed that absorption edge shifts toward shorter wavelength as the concentration of Ni increases, depicting a blue shift in band gap energy. The absorption edge shifted due to charge transfer from V.B (valence band) to C.B (conduction band) [63]. It has been observed that the absorbance can vary with some factors like oxygen deficiency, particle size and defects in material [64].

The direct band gap energy has been calculated by well known Tauc's equation [59] and its values are tabulated in Table 4. It is presented in Fig. 10 (a) and (b) respectively. The band gap energy of rutile is 3 eV [65]. It is observed that bang gap energy (E_g) increases from 3.2 eV to 3.7 eV as the Ni concentration increases. This increase in band gap energy is due to a decrease in the crystallite size as is observed in the XRD analysis. As the crystallite size decreases, the *Eg* increases, which causes the decrease in the number of overlapping energy levels. So, the gap among the valence and conduction band increases which increases the energy difference between these two bands by narrowing the band width [59]. The variation of band gap energy with dopants depends on synthesis methods, experimental conditions and types of dopants. Many research papers reported that band gap energy decreased as doping concentration of Fe increased [66,67] into TiO_2. There are also contrary reports in which the band gap energy increased

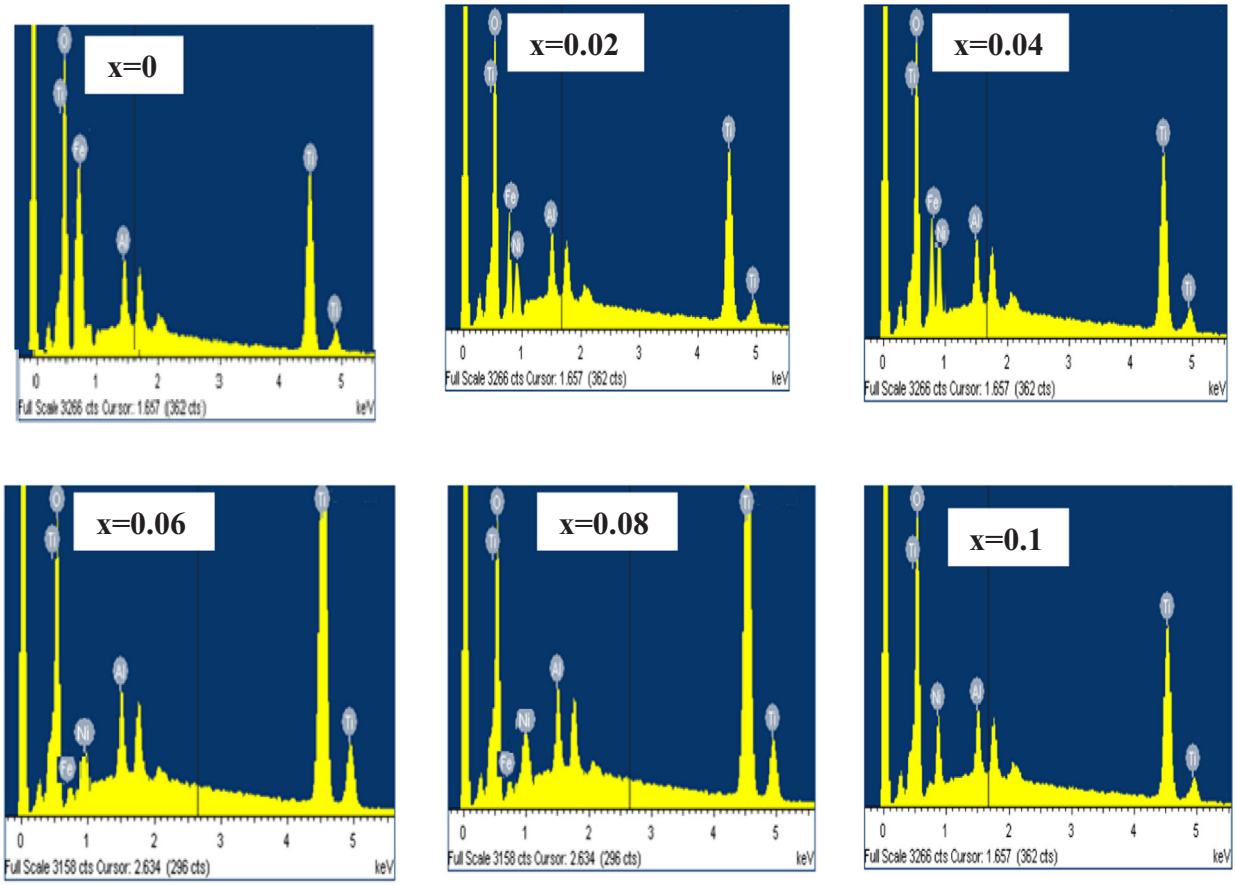

Fig. 7. EDX spectra of $Ti_{0.9}Fe_{0.1-x}Ni_xO_2$.

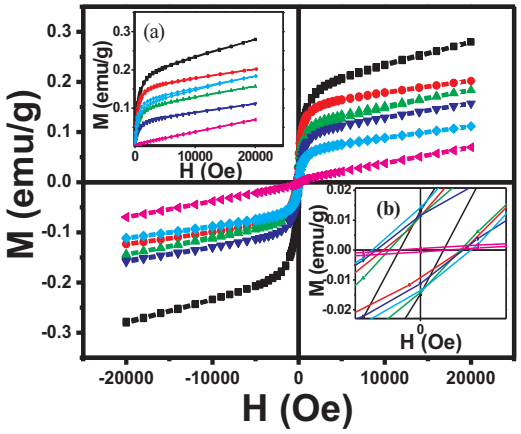

Fig. 8. M-H loops of $Ti_{0.1}Fe_{0.1-x}Ni_xO_2$ inset **(a):** decrease of magnetization with Ni inset **(b):** increase of coercivity with Ni.

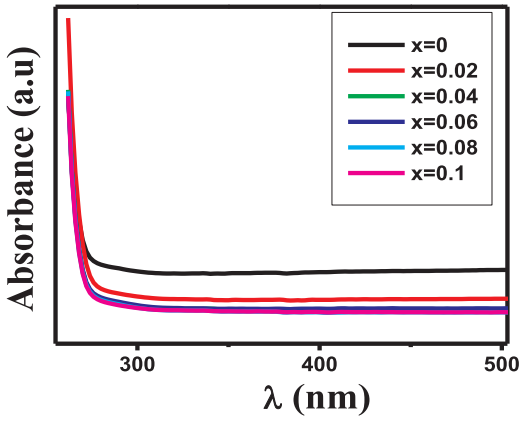

Fig. 9. UV–Vis absorption spectra of $Ti_{0.9}Fe_{0-1-x}Ni_xO_2$.

Table 3
Magnetization, coercivity and retentivity of $Ti_{0.9}Fe_{0.1-x}Ni_xO_2$.

Composition	Magnetization (M) emu/g	Coercivity Hc (O_e)	Retentivity M_r $\times 10^{-2}$
$Ti_{0.9}Fe_{0.1}O_2$	0.27	37	1.3
$Ti_{0.9}Fe_{0.08}Ni_{0.02}O_2$	0.20	66	2.9
$Ti_{0.9}Fe_{0.06}Ni_{0.04}O_2$	0.18	77	3.5
$Ti_{0.9}Fe_{0.04}Ni_{0.06}O_2$	0.16	96	1.16
$Ti_{0.9}Fe_{0.02}Ni_{0.08}O_2$	0.11	99	1.1
$Ti_{0.9}Ni_{0.1}O_2$	0.07	43	5×10^{-3}

Table 4
Band gap energy and grain size of $Ti_{0.9}Fe_{0-1-x}Ni_xO_2$.

Composition	Band gap energy (eV)	Grain size from SEM (μm)
$Ti_{0.9}Fe_{0.1}O_2$	3.20	0.51
$Ti_{0.9}Fe_{0.08}Ni_{0.02}O_2$	3.3	0.9
$Ti_{0.9}Fe_{0.06}Ni_{0.04}O_2$	3.62	1.2
$Ti_{0.9}Fe_{0.04}Ni_{0.06}O_2$	3.75	1.5
$Ti_{0.9}Fe_{0.02}Ni_{0.08}O_2$	3.75	1.7
$Ti_{0.9}Ni_{0.1}O_2$	3.8	1.8

as Fe contents increased [68,69]. T-H. Leea et al. [70] observed both increasing and decreasing trends of band gap energy with different doping concentration of Fe into TiO_2. Jianjun et al. [71] found a

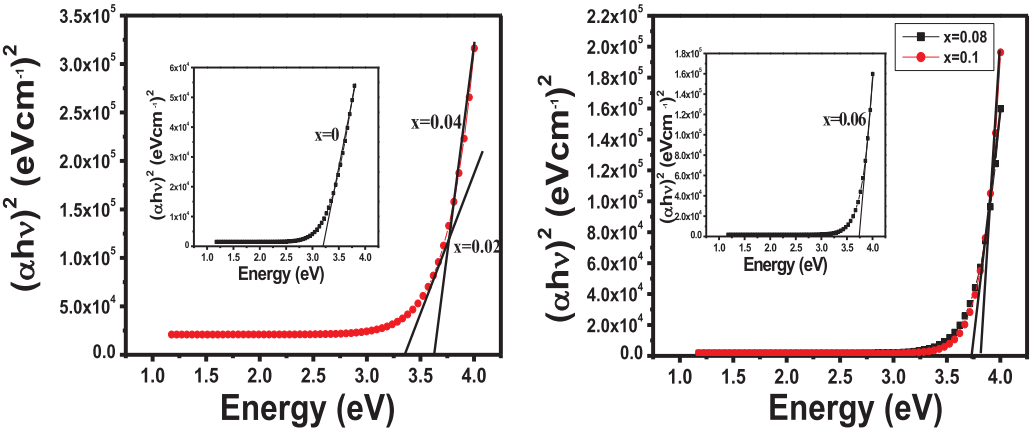

Fig. 10. Band gap energy of $Ti_{0.9}Fe_{0-1-x}Ni_xO_2$ **(a):** x = 0, 0.02, 0.04 **(b):** x = 0.06, 0.08, 0.1.

decrease in band gap energy by varying different concentrations of Ni into TiO_2 While Fe and Ni co-doped into TiO_2,decreased the band gap energy [52].

4. Conclusions

A series of $Ti_{0.9}Fe_{0-1-x}Ni_xO_2$(x = 0, 0.02, 0.04, 0.06, 0.08, 0.1) has been synthesized by the solid state reaction method. A true rutile phase is attained without any secondary impurity. A decrease in crystallite size is observed. Room temperature Raman spectra depict the presence of oxygen vacancies and defects. SEM analysis results into a denser, smoother and cracks free surface by the addition of Ni into $Ti_{0.9}Fe_{0.1}O_2$. EDX analysis shows that the contents of Fe and Ni are according to their stoichometric ratio into TiO_2. Magnetic measurements at room temperature depicts ferromagnetic behavior for all the samples. Optical properties measured by spectrophotometer reveal an increase in band gap energy from 3.2 eV to 3.8 eV. The presence of the ferromagnetism at room temperature and the crystallite size in nanocrystalline range signifies the importance of present work. These features may be useful for potential applications in memory devices with reduced dimensions

Acknowledgments

This project was funded by scholarship of HEC (Higher education commission Pakistan) through grant no. 112-33622-2PS1-529.

Conflicts of interest

There is no conflict of interest among authors. The manuscript is written and approved by all the authors.

References

[1] S.A. Ahmed, Ferromagnetism in Cr-, Fe-, and Ni-doped TiO_2 samples, J. Magn. Magn. Mater. 442 (2017) 152–157.
[2] H. Ohno, Making nonmagnetic semiconductors ferromagnetic, Science 281 (1998) 951–956.
[3] O. Mounkachi, E. salmani, M. Boujnah, H. Labrim, H. El Moussaoui, M. hamedoun, A. benyoussef, A. El Kenz, H. Ez-Zahraouy, R. masrour, E.K. Hlil, High temperature magnetic properties of nanocrystalline $Sn_{0.95}Co_{0.05}O_2$, Bull. Mater. Sci. 37 (2014) 563–569.
[4] T. Dietl, H. Ohno, F. Matsukura, J. Cibert, Z. Ferrand, Zener model description of ferromagnetism in zinc-blende magnetic semiconductors, Science 287 (2000) 1019–1022.
[5] Y. Matsumoto, Room-temperature ferromagnetism in transparent transition metal-doped titanium dioxide, Science 291 (2001) 854–856.
[6] A.J. Silvestre, S. Rout, S. Dalui, L.C.J. Pereira, A.S. Viana, O. Conde, Co and (Co, Mo) doping effects on the properties of highly reduced TiO_2 anatase thin films, Curr. Appl. Phys. 17 (2017) 174–180.
[7] J. Winkler, Titanium Dioxide: Production, Properties and Effective Usage, second revised ed., VincentzNetwork, Hannover, 2013.
[8] K. Nakata, A. Fujishima, TiO_2 photocatalysis: design and applications, J. Photochem. Photobiol. C. Photochem. Rev. 13 (2012) 169–189.
[9] K. Hashimoto, H. Irie, A. Fujishima, TiO_2 photocatalyst: a historical overview and future prospectus, Jpn. J. Appl. Phys. 44 (2005) 8269–8285.
[10] S. Chatterjee, K.J. Bhattacharyya, Photocatalytic properties of one-dimensional nanostructured titanates, Phys. Chem. C 114 (2010) 9424–9430.
[11] Y. Ohko, S. Saitoh, T. Tatsuma, A. Fujishima, Photoelectrochemical anticorrosion and self-cleaning effects of a TiO_2 coating for type 304 stainless steel, J. Electrochem. Soc. 148 (2001) B24–B28.
[12] F.A. Akin, H. Zreiqat, S. Jordan, M.B.J. Wijesundara, L. Hanley, Preparation and analysis of macroporous TiO_2 films on Ti surfaces for bone–tissue implants, J. Biomed. Mater. Res. 57 (2001) 588–596.
[13] M. Lorenzetti, D. Biglino, S. Novak, S. Kobe, Photoinduced. properties of nano-crystalline TiO_2 anatase coating on Ti-based bone implants, Mater. Sci. Eng. C 37 (2014) 390–398.
[14] D.S. Jeong, H. Schroeder, R. Waser, Resistive switching in TiO_2 thin films, Electrochem. Sol. State Lett. 10 (2007) G51–G53.
[15] D.B. Strukov, G.S. Snider, D.R. Stewart, R.S. Williams, The missing memristor found, Nature 453 (2008) 80–83.
[16] W. Cai, T. Schmidt, U. Jeorges, F. Ellinger, Nanoscale memristor device as synapse in neuromorphic systems, IEEE Trans. Circ. Syst. 59 (2012) 2405–2412.
[17] S. Liu, Z. Wang, C. Yu, H.B. Wu, G. Wang, Q. Dong, J. Qiu, A. Eychmüller, X.W. Lou, A flexible TiO_2(B)-based battery electrode with superior power rate and ultralong cycle life, Adv. Mater. 25 (2013) 3462–3467.
[18] Z.H. Chen, I. Belharouak, Y.K. Sun, K. Amine, Titanium-based anode materials for safe lithium-ion batteries, Adv. Funct. Mater. 23 (2013) 959–969.
[19] B. O'Regan, M. Gr€atzel, A low-cost, high efficiency solarcell based on dye-sensitized colloidal TiO_2 films, Nature 353 (1991) 737–740.
[20] J.T. Park, W.S. Chi, S.J. Kim, D. Lee, J.H. Kim, Mesoporous TiO_2 Bragg stack templated by graft copolymer fordye-sensitized solar cells, Sci. Rep. 4 (2014) 1–7.
[21] Y.H. Zhang, A. Reller, Nanocrystalline iron-doped mesoporous titania and its phase transition, J. Mater. Chem. 11 (2001) 2537–2541.
[22] M. Hirano, T. Joji, M. Inagaki, H. Iwata, Direct formation of iron(III)-doped titanium oxide (anatase) by thermal hydrolysis and its structural property, J. Am. Ceram. Soc. 87 (35) (2004) 35–41.
[23] N. Perkas, O. Palchik, I. Brukental, I. Nowik, Y. Gofer, Y. Koltypin, A. Gedanken, A mesoporous iron–titanium oxide composite prepared sonochemically, J. Phys. Chem. B 107 (2003) 8772–8778.
[24] A. Takeda, T. Sato, C. Kaito, S. Kaneko, Structure of metal doped TiO_2 particles produced by RF plasma, Thin Solid. Films 435 (2003) 211–215.
[25] R. Alexandrescu, I. Morjan, M. Scarisoreanu, R. Birjega, E. Popovici, I. Soare, L. Gavrila-Florescu, V.I. Sandu, F. Dumitrache, G. Prodan, E. Vasile, E. Figgemeier, Structural investigations on TiO_2 and Fe-doped TiO_2 nanoparticles synthesized by laser pyrolysis, Thin Solid. Films 515 (2007) 8438–8445.
[26] X. Zhang, M. Zhou, L. Lei, Co-deposition of photocatalytic Fe doped TiO_2 coatings by MOCVD, Catal. Commun. 7 (2006) 427–431.
[27] H. Yamashita, M. Harada, J. Misaka, M. Takeuchi, B. Neppolian, M. Anpo, Photocatalytic degradation of organic compounds diluted in water using visible light-responsive metal ion-implanted TiO_2 catalysts: Fe ion-implanted TiO_2, Catal. Today 84 (2003) 191–196.
[28] F. Gracia, J.P. Holgado, F. Yubero, A.R. Felipe, Structural, optical, and photoelectrochemical properties of Mn^{+} - TiO2 model thin film photocatalyst, J. Phys. Chem. B 108 (2004) 17466–17476.
[29] L.T. Tseng, X. Luo, N. Bao, J. Ding, S. Li, J. Yi, Structures and properties of transition-metal-doped TiO_2 nanorods, Mater. Lett. 170 (2016) 142–146.
[30] M. Li, J. He, Synthesis and room-temperature ferromagnetism of porous V-doped rutile TiO_2 microspheres, Mater. Lett. 174 (2016) 48–52.
[31] L. Mustafa, S. Anjum, S. Waseem, S. Javed, S.M. Ramay, S. Attiq, Effect of Co and Ni co-doping on the structural, magnetic, electrical and optical properties of ZnO, Mater. Res. Bull. 84 (2016) 32–38.
[32] Z. Zou, Z. Zhou, H. Wang, M. Du, Oxygen defect-mediated magnetism in Fe-C co-doped TiO_2, Mater. Sci. Eng., B. 2016 (2016) 1–7.
[33] X.J. Wang, Y.L. Song, L.L. Tao, et al., Origin of ferromagnetism in aluminum-doped

TiO_2thin films: theory and experiments, Appl. Phys. Lett. 105 (2014) 262402.
[34] K. Srinivas, P. Venugopal Reddy, Synthesis, structural, and magnetic properties of nanocrystalline $Ti0.95Co_{0.0}5O_2$-diluted magnetic semiconductors, J. Supercond. Nov. Magn. 27 (2014) 2521–2538.
[35] R. Amraouia, M. Doghmanea, S. Chettibia, D.F. Laeferb, The electronic structure and optical properties of rutile TiO_2 codoped with nickel and cerium, Chin. J. Phys. 55 (2017) 2393–2399.
[36] D. Chen, Z. Jiang, J. Geng, Q. Wang, D. Yang, Carbon and nitrogen co-doped TiO_2 with enhanced visible-light photocatalytic activity, Ind. Eng. Chem. Res. 46 (2007) 2741–2746.
[37] C. Liu, X. Tang, C. Mo, Z. Qiang, Characterization and activity of visible-light-driven TiO_2 photocatalyst codoped with nitrogen and cerium, J. Solid State Chem. 181 (2008) 913–919.
[38] Y. Zhang, Y. Shen, F. Gu, M. Wu, Y. Xie, J. Zhang, Influence of Fe ions in characteristics and optical properties of mesoporous titanium oxide thin films, Appl. Surf. Sci. 256 (2009) 85–89.
[39] Y. Matsumoto, M. Murakami, T. Shono, T. Hasegawa, T. Fukumura, M. Kawasaki, P. Ahmet, T. Chikyow, S.Y. Koshihara, H. Koinuma, Room-temperature ferromagnetism in transparent transition metal-doped titanium dioxide, Science 291 (2001) 854–856.
[40] S.A. Chambers, S. Thevuthasan, R.F.C. Farrow, R.F. Marks, J.U. Thiele, L. Folks, M.G. Samant, A.J. Kellock, N. Ruzycki, D.L. Ederer, U. Diebold, Epitaxial growth and properties of ferromagnetic co-doped TiO_2 anatase, Appl. Phys. Lett. 79 (2001) 3467–3469.
[41] J. Tian, H. Gao, H. Deng, L. Sun, H. Kong, P. Yang, J. Chu, Structural, magnetic and optical properties of Ni-doped TiO_2 thin films deposited on silicon(100) substrates by sol–gel process, J. Alloy. Compd. 581 (2013) 318–323.
[42] Y.L. Zhao, M. Motapothula, N.L. Yakovlev, Z.Q. Liu, S. Dhar, A. Rusydi, Ariando, M.B.H. Breese, Q. Wang, T. Venkatesan, Reversible ferromagnetism in rutile TiO_2 single crystals induced by nickel impurities, Appl. Phys. Lett. 101 (2012) 142105.
[43] N. Bahadur, R. Pasricha, Govind, S. Chand, R.K. Kotnala, Effect of Ni doping on the microstructure and high Curie temperature ferromagnetism in sol–gel derived titania powders, Mater. Chem. Phys. 133 (2012) 471–479.
[44] S. Waseem, S. Anjum, L. Mustafa, T. Zeeshan, R. Zia, N. Mohsin, Absence of room temperature ferromagnetism in Co and Cr co-doped Tio_2 based dilute magnetic semiconductors, Dig. J. Nanomater. 2 (2016) 411–418.
[45] K. Siddhapara, D. Shah, Characterization of nanocrystalline cobalt doped TiO_2 sol–gel material, J. Cryst. Growth 352 (2012) 224–228.
[46] B. Parveen, M. Hassan, S. Atiq, S. Riaz, S. Naseem, M.A. Toseef, Structural and dielectric study of nano-crystalline single phase $Sn1-xNixS$ ($xNi = 0–10\%$) showing room temperature ferromagnetism, Prog. Nat. Sci. Mater. 27 (2017) 303–310.
[47] S. Waseem, S. Anjum, L. Mustafa, A. Dar, F. Bashir, R. Zia, Effects of Cr and Fe co-doping on structural, optical, electrical and magnetic properties of titanium dioxide (TiO_2), Mater. Sci. Pol. 33 (2015) 508–514.
[48] M. Saleem, S.A. Siddiqi, S. Atiq, M.S. Anwar, S. Riaz, Room temperature magnetic behavior of sol-gel synthesized Mn doped ZnO, Chin. Phys. Lett. 29 (2012).
[49] X. Jian-Ping, L. Lan, L. Li-Ya, Z. Xiao-Song, C. Xi-Ming, W. Jian-Feng, D. You-Wei, Structural and magnetic properties of Fe-doped anatase TiO_2 fiiO_2annealed in vacuum, Chin. Phys. Lett. 26 (2009) 097502.
[50] S. Anjum, H. Nazli, R. Khurram, T. Zeeshan, S. Riaz, A. Usman, Role of Zn substitution on structural, magnetic and dielectric properties of Cu–Cr spinel ferrites, Indian J. Phys. 90 (2016) 869–880.
[51] S.A. Ahmed, Annealing effects on structure and magnetic properties of Mn-doped TiO_2, J. Magn. Magn. Mater. 402 (2016) 178–183.
[52] T. Sun, J. Fan, E. Liu, L. Liu, Y. Wang, H. Dai, Y. Yang, W. Hou, X. Hu, Z. Jiang, Fe and Ni co-doped TiO_2 nanoparticles prepared by alcohal - thermal method: application in hydrogen evolution by water splitting under visible light irradiation, Powder Technol. 228 (2012) 210–218.
[53] M. Reghima, A. Akkari, C. Guasch, N. Turki-Kamoun, Structural, optical, and electrical properties of SnS: Ag thin films, J. Appl. Phys. 7 (2015) 4392–4399.
[54] H. Wang, J. Wei, R. Xiong, J. Shi, Enhanced ferromagnetic properties of Fe+ N codoped TiO_2 anatase, J. Magn. Magn. Mater. 324 (2012) 2057–2061.
[55] F. Hardcastle, Raman spectroscopy of titania (TiO_2) nanotubular water-splitting catalysts, J. Ark. Acad. Sci. 65 (2011) 43–48.
[56] T. Ohsaka, F. Izumi, Y. Fujiki, Raman spectrum of anatase TiO_2, J. Raman Spectrosc. 7 (1978) 321–324.
[57] G. Xing-Yuan, X. Da-Peng1, D. Zhan-Hui, S. Wen-Hui, Preparation and Raman spectrum of rutile single crystals using floating zone method, Chin. Phys. Lett. 23 (6) (1645) 2006.
[58] B. Santara, B. Pal, P. Giri, Signature of strong ferromagnetism and optical properties of Co doped TiO_2 nanoparticles, J. Appl. Phys. 110 (11) (2011) 114322.
[59] L. Mustafa, S. Anjum, S. Waseem, R. Zia, R. Choudhry, S.M. Ramay, A. Mahmood, S. Attiq, S. U-D Khan, Investigation of structural, magnetic, and optical properties of ZnO Codoped with Co and Cd, Adv. Condens. Matter Phys. 2014 (2014) 1–6.
[60] A.M. Al-Saie, A. Al-Shater, S. Arekat, A. Jaffar, M. Bououdina, Effect of annealing on the structure and magnetic properties of mechanically milled TiO_2–Fe_2O_3 mixture, Ceram. Int. 39 (2013) 3803–3808.
[61] A.K. Das, M. Kar, A. Srinivasan, Room temperature ferromagnetism in undoped ZnO nanofibers prepared by electrospinning, Phys. B: Condens. Matter 448 (2014) 112–114.
[62] R. Khaibullin, L. Tagirov, B. Rameev, S. Ibragimov, F. Yıldız, B. Akta, High Curie temperature ferromagnetism in cobalt-implanted single-crystalline rutile, J. Phys. Condens. Matter 16 (2004) L443–L449.
[63] S. Patel, S. Kurian, N.S. Gajbhiye, Room-temperature ferromagnetism of Fe-doped TiO_2 nanoparticles driven by oxygen vacancy, Mater. Res. Bull. 48 (2013) 655–660 (655 - 660).
[64] S. Fabbiyola, L.J. Kennedy, T. Ratnaji, J.J. Vijaya, U. Aruldoss, M. Bououdina, Effect of Fe-doping on the structural, optical and magnetic properties of ZnO nanostructures synthesized by co-precipitation method, Ceram. Int. 42 (2016) 1588–1596.
[65] Y. Yang, W. Zhou, Y. Liang, L. Liu, P. Wu, Tuning band gap and ferromagnetism in epitaxial Al-doped SnO_2 films by defect engineering, J. Cryst. Growth 430 (2015) 75–79 (2015).
[66] A.P. Singh, S. Kumari, R. Shrivastav, S. Dass, V.R. Satsangi, Iron doped nanostructured TiO_2 for photoelectrochemical generation of Hydrogen, Int. J. Hydrog. Energy 33 (2008) 5363–5368.
[67] J. Zhua, F. Chen, J. Zhang, H. Chen, M. Anpo, Fe+3_TiO_2 photocatalysis prepared by combining sol-gel method with hydrothermal treatment and their characterization, J. Photochem. Photobiol. A: Chem. 180 (2006) 196–204.2.
[68] N. Farhangi, R.R. Chowdhury, Y.M. Gonzalez, M.B. Ray, P.A. Charpentier, Visible light active Fe doped TiO_2nanowires grown on grephene using supercritical CO_2, Appl. Catal. B: Environ. 110 (2011) 25–32.
[69] D.H. Kim, H.S. Hong, S.J. Kim, J.S. Singh, K.S. Lee, photocatalytic behaviors and structural characterization of nanocrystalline Fe- doped TiO_2 synthesized by chemical alloying, J. Alloy. Compd. 375 (2004) 259–264.
[70] T.-H. Leea, H. Ryu, W.-J. Lee, Photoelectrochemical properties of iron(III)-doped TiO_2nanorods, Ceram. Int. 41 (2015) 7582–7589.
[71] J. Tian, H. Gao, H. Deng, L. Sun, H. Kong, P. Yang, J. Chu, Structural, magnetic and optical properties of Ni-doped TiO2 thin films deposited on silicon(100) substrates by sol–gel process, J. Alloy. Compd. 581 (2013) 318–323.